

Programmable branched flow of light

Shan-shan Chang^{1,2}, Daxing Xiong³, Ze-huan Zheng¹, Li-Wei Wang^{4,5}, Yan-qing Lu^{6,*}
 Lu-Jian Chen^{7,†}, Jian-Hua Jiang^{4,5,‡} and Jin-hui Chen^{1,2§}

¹*Institute of Electromagnetics and Acoustics, Key Laboratory of Electromagnetic Wave Science and Detection Technology, Xiamen University, Xiamen 361005, China*

²*Shenzhen Research Institute of Xiamen University, Shenzhen 518000, China*

³*MinJiang Collaborative Center for Theoretical Physics,*

College of Physics and Electronic Information Engineering, Minjiang University, Fuzhou 350108, China

⁴*State Key Laboratory of Bioinspired Interfacial Materials Science, Suzhou Institute for Advanced Research, University of Science and Technology of China, Suzhou 215123, China*

⁵*School of Physical Sciences, University of Science and Technology of China, Hefei 230026, China*

⁶*College of Engineering and Applied Sciences, Nanjing University, Nanjing, 210023, China*

⁷*Department of Electronic Engineering, Xiamen University, Xiamen 361005, China*

(Dated: January 21, 2026)

We demonstrate deterministic control of branched flow of light using anisotropic nematic liquid crystals. By sculpting the director field via photoalignment, we create spatially programmable optical potentials that govern light scattering and propagation. This platform enables configurable, anisotropic branched flow of light and reveals a universal scaling law for its characteristic features, directly connecting disordered photonics with mesoscopic wave transport. Under extreme anisotropy, we observe a pronounced directional channeling effect, driven by anomalous symmetry-breaking velocity diffusion, which concentrates light propagation along preferential directions while suppressing transverse spreading. These findings establish a tunable material platform for harnessing branched flow of light, opening pathways toward on-chip photonic circuits that exploit disorder-guided transport, scattering-resilient endoscopic imaging, and adaptive optical interfaces in complex media.

The propagation of light through disordered media spans a rich spectrum of physical regimes, from ballistic transport in homogeneous media to fully diffusive spreading under strong multiple scattering. Between these extremes lies a fascinating intermediate regime where coherent interference in weakly correlated disordered potentials gives rise to a remarkable phenomenon: the branched flow of light [1, 2]. Here, light spontaneously organizes into intense, filamentary channels that persistently branch during propagation, forming patterns reminiscent of river networks or lightning strikes. This behavior emerges universally across wave systems—from electrons and microwaves to water waves and light—when the correlation length of the disorder exceeds the wavelength [3–5]. First discovered in two-dimensional electron gases [6–9], branched flow has since been observed in optical systems such as thin soap films [1] and tailored photonic platforms [10, 11]. However, experimental studies have remained largely observational, with limited ability to control or program the branching process. Crucially, key regimes such as anisotropic branched flow have remained virtually unexplored, while the lack of a programmable material platform has hindered the transition from fundamental observation to functional applications.

Theoretical insights suggest that anisotropy in the disordered potential offers a powerful tool to tailor branched flows [12, 13]. For instance, anisotropic landscapes such as seabed topography can channel tsunami waves into extreme, rogue-wave-like amplitudes [14, 15]. Understanding and harnessing such anisotropic branching is thus essential for predicting and controlling extreme wave events

in fields ranging from nonlinear optics to hydrodynamics and acoustics [16–18]. Moreover, the ability to program branched flow of light—to dictate where, when, and how branches form—would open transformative opportunities in photonic technology. A reconfigurable platform capable of on-demand optical channeling could enable reprogrammable photonic circuits that guide light along dynamically tunable pathways, robust endoscopic imaging through scattering biological tissues, and adaptive optical interfaces that control light–matter interaction in complex media. Realizing such applications demands a material that combines precise spatial control over the disorder potential with notable stability—a combination that has remained elusive.

In this work, we introduce a programmable material platform that achieves deterministic control over branched light flow by leveraging the tunable anisotropy and microscale patterning capability of nematic liquid crystals (NLCs) [19–24]. Using high-resolution photoalignment, we engineer spatially correlated disorder with continuous and adjustable anisotropy, creating optical potentials that are both smooth and fully reconfigurable. This approach transforms branched flow from a passively observed phenomenon into an actively controllable wave-transport effect. With this platform, we experimentally demonstrate on-demand customization of branching morphology, validate a universal scaling law for anisotropic branched flow, and uncover a previously unreported regime of anomalous velocity diffusion under extreme anisotropy. The latter leads to a pronounced directional channeling effect, effectively guiding light along

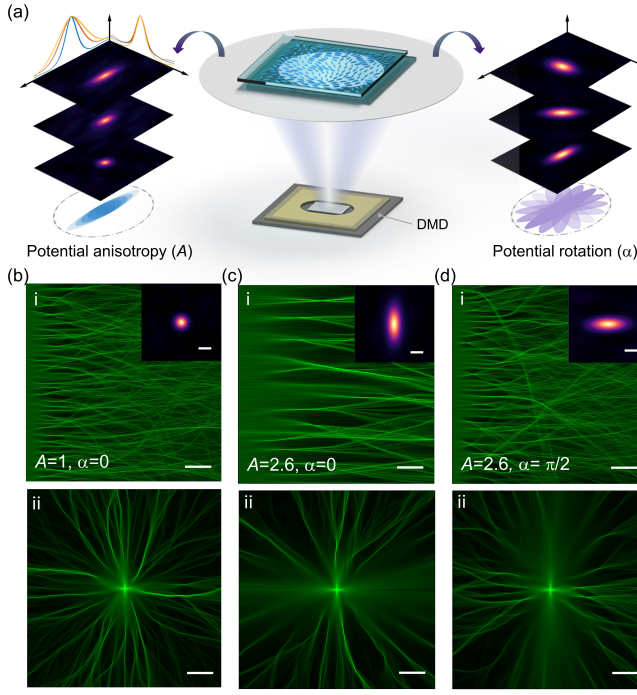


FIG. 1. Programmable optical branched flow in nematic liquid crystals (NLC). (a) Tailoring disordered potential of photo-alignment NLC film via potential anisotropy and rotation for controlling anisotropic branched flow. DMD: digital micro-mirror device. (b-d) The simulated optical branched flow fields in the anisotropic disordered NLC film with different potential anisotropy (A) and rotation (α). The panels (i) are the simulated branched flow fields with a plane-wave excitation, where the insets show the correlation function of the corresponding disordered potential. The panels (ii) are the simulated branched flow fields via a point-source excitation. Here the correlation length l_x is set constant as 15 μm . All the scale bars are 200 μm .

designer pathways without the need for conventional waveguides. Our work not only provides a fundamental breakthrough in the control of wave propagation in disordered media, but also establishes a versatile platform for applications in on-chip photonics, biomedical imaging, and adaptive optical systems.

In our platform, the NLC film serves as a slab waveguide that effectively supports guided light propagation and enables us to study branched flow of light. The propagation of the guided extraordinary light wave (e -wave) is governed by the spatial distribution of the director field $\hat{\mathbf{n}}(x, y)$ of the liquid crystal molecules, which determines the effective refractive index distribution $n_{\text{eff}}(x, y)$ felt by the e -wave [25]. The thickness of the implemented NLC film (20 μm) is much larger than the wavelength of the laser light (532 nm) used in our experiments, and thus the waveguide-induced effective index change is neglected [10]. The equation governing the propagation of a monochromatic light in the NLC film is approximately 2D Helmholtz equation, which is written in a form re-

sembling the time-independent Schrödinger equation,

$$-\nabla^2\psi + V(x, y)\psi = k_0^2\bar{n}^2\psi, \quad (1)$$

where ψ is the light wave amplitude and $V(x, y)$ is the effective optical potential given by (see Supplementary Material for details)[2, 10, 26, 27]:

$$V(x, y) = k_0^2(\bar{n}^2 - n_{\text{eff}}(x, y)^2), \quad (2)$$

where k_0 is the wavevector of the laser light in vacuum, $\bar{n} = \sqrt{\langle n_{\text{eff}}^2(x, y) \rangle}$ is the (root-mean-square) averaged refractive index in the observation area of the NLC film. The average optical potential is $\langle V(x, y) \rangle \equiv 0$, indicating purely the effect of the spatial fluctuation of potentials. Physically, $V(x, y)$ gives a smooth, spatially varying disordered potential that scatters the light and results in the branched flows. The spatial correlation of the optical potential $c(x', y') = \langle V(x', y')V(0) \rangle$ is a quantity that governs the key properties of the branched flow of light [1, 3, 28]. For instance, in an isotropic medium, the correlation function of the disordered optical potential always falls into the form, $c(x', y') = \epsilon^2 f((x'^2 + y'^2)/l_c^2)$, where $f(\cdot)$ is a dimensionless form function. The first-branch distance d_f —the characteristic length scale of branched flows—is defined as the statistically averaged distance from the plane-wave source to the first caustic focusing positions. d_f is determined by the correlation length l_c and relative strength ϵ of the disordered potential.

Theoretically, the position of the first caustic, or the first-branch distance, obeys a generalized relation in anisotropic disordered potentials (see Supplementary Material for details) [12, 27]:

$$d_f \propto \epsilon^{-2/3} (l_y^4/l_x)^{1/3} = \epsilon^{-2/3} A^{4/3} l_x, \quad (3)$$

where l_x and l_y are the correlation length along the longitudinal and transverse directions, respectively, $A = l_y/l_x$ is the potential anisotropy. In a more general anisotropic disordered medium, where the principal axis is tilted by an angle α relative to the x -direction, the angular dependence of the first-branch distance can be obtained:

$$d_f \propto \epsilon^{-2/3} A^{4/3} l_x (\cos^2 \alpha + \sin^2 \alpha/A^2)^{5/6} \quad (4)$$

In the experiment, by tailoring director distribution of NLC films to construct anisotropic disordered potentials using the photoalignment technique (Fig. 1a) [24, 29–31], the branched flow of light can be programmed and controlled on demand.

The disordered optical potential is generated by convolving a 2D random matrix with Gaussian white noise and the target anisotropic correlation function (see Supplementary Material for details [27]). Since branched flow arises from random small-angle deflection events induced by a weakly correlated potential, the input light source

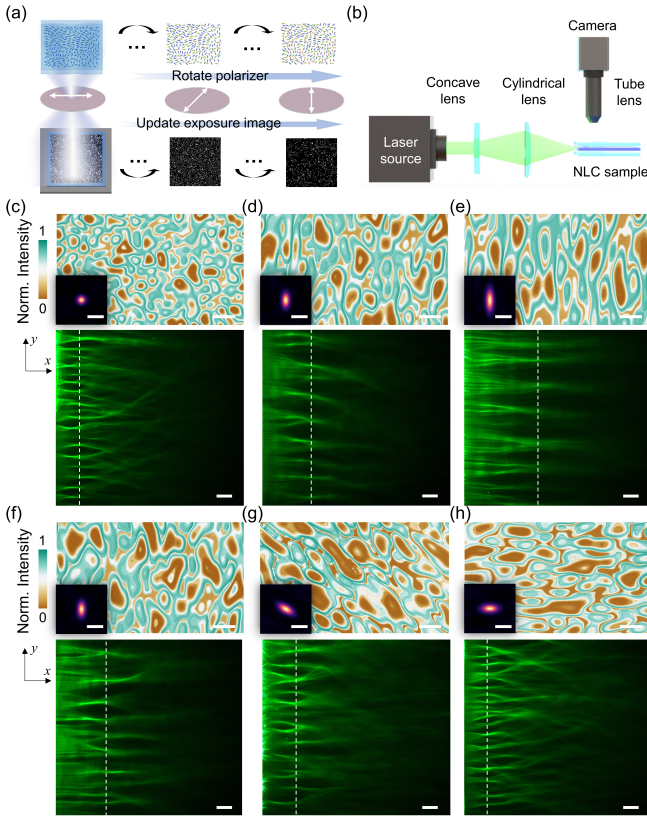


FIG. 2. Experimental observation of anisotropic branched flow with controllable first-branch distance. (a) Schematic diagram of photo-patterning NLC films with designed disordered director distributions. (b) Experimental setup for excitation and characterization of branched flow in an NLC sample. (c-h) Cross-polarized microscope images (upper panels) of fabricated NLC films with varying potential anisotropy A and potential rotation angle α , and their correspondingly measured profiles of the propagating field (lower panels). In (c-e) the disordered potentials are of the same $\alpha = 0$, and different A -values: (c) $A = 1.0$, (d) $A = 1.8$. (e) $A = 2.6$. In (f-h) the disordered potentials are of the same $A = 1.8$, and different α -values: (f) $\alpha = 0$, (g) $\alpha = \pi/4$, (h) $\alpha = \pi/2$. The insets in the upper panels of (c-h) are the autocorrelation function of the disordered optical potential. The white dashed line in lower panels of (c-h) indicates the measured first-branch distance. All the scale bar is 100 μm .

is required to be weakly localized in phase space, such as a plane-wave source [32]. The simulated branched light fields under plane-wave illumination (Figs. 1b-d, panels i) align well with the theoretical scaling law for the first-branch distance d_f . For example, d_f for $(A = 1, \alpha = 0)$ is smaller than for $(A = 2.6, \alpha = 0)$, while d_f for $(A = 2.6, \alpha = 0)$ exceeds that for $(A = 2.6, \alpha = \pi/2)$. We also simulate light propagation with a point-source excitation (panels ii of Figs. 1b-d), which reveals a strong polar angle dependence of the wave caustics distribution in anisotropic potentials. Furthermore, a self-channeling effect emerges along a direction where the correlation of

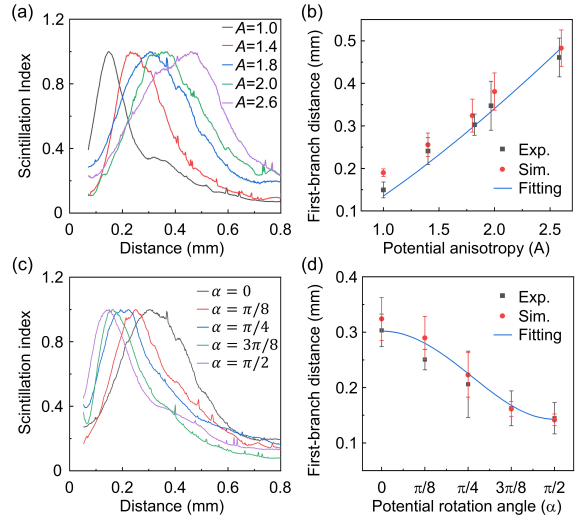


FIG. 3. Quantitative measurement of the first-branch distance on potential anisotropy and potential rotation. (a) The shift of scintillation index curves on varying potential anisotropy. (b) Experimental and simulated results of first-branch distance depending on potential anisotropy. (c) The shift of scintillation index curves on varying potential rotation angle. The potential anisotropy is set as 1.8. (d) Experimental and simulated results of first-branch distance depending on potential rotation angle. The error bars in (b,d) is bandwidth of 98% peak value of the normalized scintillation index curve.

the disorder potential is strong, consistent with the previous theoretical predictions [12]. These properties are examined in detail in the following sections.

To realize an effective optical potential for anisotropic branched flow, we first fabricate inhomogeneously aligned NLC films. The director distribution is digitized into 18 gray levels, corresponding to NLC director angles ranging from 0 to $17\pi/18$ radians in steps of $\pi/18$ (see Supplementary Material for details [27]). This fine discretizations of NLC directors suppress the externally angular dispersion effect of e -wave in the NLCs (see Supplementary Material for details [27]). The designed NLC films are fabricated using the photoalignment technique, where the NLC director profile is created through a multi-step partial ultraviolet exposure combined with synchronous rotation of the linear polarizer as illustrated in Fig. 2a. Experimentally, we primarily vary the anisotropy A and the rotation angle α of the disordered potential. The resulting parameter sets (ϵ, A, α) for the fabricated films are summarized (see Supplementary Material for details [27]). The optical potential strength ϵ is approximately 0.05, as determined from the birefringence of the E7 mixture ($\Delta n = 0.22$ in the visible range) [10, 29]. To characterize the emergence of the first-branch distance, we couple a quasi-plane-wave light into the NLC film and directly observe the in-plane propagating light field using a home-made optical microscope (Fig. 2b). This

far-field measurement scheme is enabled by the intrinsic weak light scattering out of the NLC film plane [25, 33].

The emergent disordered textures are verified with cross-polarized optical microscopy (upper panels of Figs. 2c–h). Furthermore, spatial variations in correlation length and potential strength are characterized in different sections within a single NLC film, revealing good self-similarity for the observation of branched flow of light (see Supplementary Material for details [27]). From the lower panels of Figs. 2(c–e), the incident light evolves from an initially uniform intensity distribution to pronounced caustics at a characteristic position d_f (approximately the first-branch distance [1, 2]). The caustic distance increases monotonously with the anisotropy of the disordered potential due to the increase in the correlation length along the y -direction. In contrast, at a fixed anisotropy ($A = 1.8$), the caustic distance decreases with increasing rotation angle in the range of $0 \sim \pi/2$ (Figs. 2f–h). This pronounced dependence on propagation angle originates from the variations in the effective transverse correlation length.

Figure 3a presents the measured scintillation index curves for five groups of samples with various potential anisotropy. Each curve represents an ensemble average over approximately ten independent realizations, in which the NLC films are designed and fabricated to have nearly identical statistical parameters (ϵ, A, α). This is enabled by the precisely engineered disordered potential via high-accuracy photoalignment. The high programmability of NLC platform is essential for achieving meaningful ensemble averaging. The scintillation index is defined as the normalized variance of the lateral light intensity: $S(x) = \langle I^2(x) \rangle / \langle I(x) \rangle^2 - 1$, where averaging is performed over the transverse y -direction and across different realizations [1, 10, 34]. Physically, $S(x)$ reaches its maximum when the transverse intensity fluctuations are strongest, marking the onset of the branching. The experimentally measured first-branch distance d_f shows quantitative agreement with both the analytical scaling law from equation (3) and numerical simulations (see Supplementary Material for details [27]). Furthermore, the measured d_f strongly depends on the potential rotation angle, closely following the theoretical predictions (Figs. 3c–d). Counterintuitively, in the polar representation (d_f, α), the angular dependence does not exhibit a simple ellipse but instead shows a distinct “peanut” shape (see Supplementary Material for details [27]). These results provide a direct experimental discovery of the universal scaling law for anisotropic branched flow.

In an isotropic disordered potential, the light field landscape excited by a point light source exhibits a branched caustic pattern that is essentially independent of the propagation angle (see Supplementary Material for details [27]). In contrast, anisotropic disordered potentials tend to concentrate optical caustics along the longer

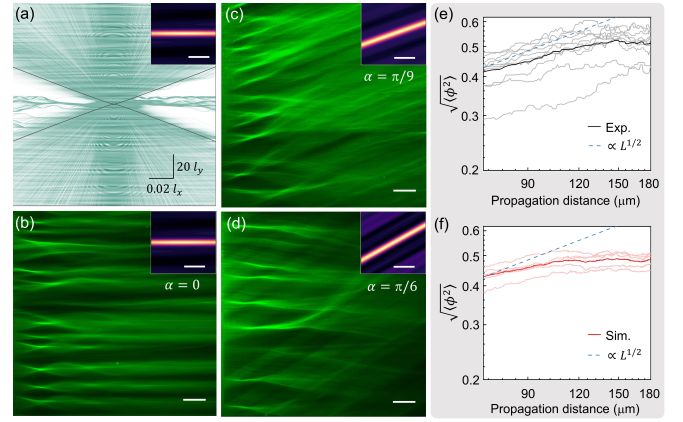


FIG. 4. Observation of light channeling effect in extreme anisotropic disordered potential. (a) Simulated branched flow field in spatially anisotropic disordered NLC films, with anisotropy of $A = 1/1000$. Here l_y is set as $16 \mu\text{m}$. The scale bar is represented by the correlation lengths. (b-d) The microscope images show the branching of a wide elliptical laser beam propagating through extreme anisotropic potentials ($A = 1/1000$) at spatial orientation angles of (b) 0 , (c) $\pi/9$, and (d) $\pi/6$. The insets in (a-d) show the autocorrelation function of the disordered potential. The scale bar is $100 \mu\text{m}$. (e-f) The standard deviation of the velocity angle for propagating light in an extremely anisotropic potential ($A = 1/1000$): (e) experimental results, (f) simulated results. The undertint curves are examples of realizations as an illustration for the typical variation in individual realizations of the disordered NLCs. The dashed-blue lines in (e-f) are proportional to $L^{1/2}$ for normal diffusion process, where L is the propagation distance.

correlation length (panels ii of Figs. 1c–d) [12]. In experiment, when excited with a narrow Gaussian beam, the self-channeling effect is enhanced with increasing potential anisotropy (see Supplementary Material for details [27]). This effect is particularly pronounced in extremely spatially anisotropic media. For example, at $l_x : l_y = 1000$ or $A=1/1000$, (Fig. 4a), the light field can be strongly localized around the x -axis, corresponding to the direction of the longer correlation length. Therefore, this light channeling regime can be shifted by simply rotating the potential (see Supplementary Material for details [27]).

For such an extremely anisotropic case ($A \ll 1$ or $l_y \ll l_x$), the disordered potential distribution is only weakly dependent on the x -coordinate. Therefore, the energy exchange can be approximated as occurring solely in the y -direction, i.e., $E_{total} = E_y + U(y)$. When all kinetic energy is converted into potential energy, i.e., $U = v_0^2 \sin^2 \beta / 2$, the transverse component of the light’s trajectory reverses direction, while the longitudinal (x) propagation remains monotonic. According to the Piterbarg’s theorem [12, 35], the maximum lateral excursion y_m is related to the peak potential via $U_{max} = \epsilon \sqrt{2 \ln(y_m/l_c) + 2}$. Along with $U_{max} = v_0^2 \sin^2 \beta / 2$, the

asymptotic curve for optical localization is obtained, shown as the black line in Fig. 4a. Most of the light caustics are confined within the cone-like region, producing a nontrivial optical channeling effect.

To probe light localization, we imprint the designed, extremely anisotropic disordered potential onto the NLC director field via photo-alignment and launch a quasi-plane wave into samples with varying potential rotation angles α . For small rotation angles $\alpha \leq \pi/9$, the resulting caustics remain tightly confined along the principal axis of the potential (Figs. 4b–c), exhibiting a pronounced waveguiding-like behavior (see Supplementary Material [27] for additional data). In contrast, when α reaches $\pi/6$ —slightly exceeding the theoretical asymptotic angle—the emergent caustics no longer align with the potential’s principal axis. Instead, they persist along the initial propagation direction (Fig. 4d). These experimental observations are in excellent agreement with the theoretical profile shown in Fig. 4a.

To elucidate how spatial anisotropy governs light localization, we analyze the diffusion of velocity angles during the light propagation in an extremely spatially anisotropic potential ($A = 1/1000$, $\alpha = 0$). We experimentally and numerically evaluate the dependence of the velocity-angle standard deviation, $\sqrt{\langle \phi^2 \rangle(x)}$, on the propagation distance L , as shown in Fig. 4e–f (see Supplementary Material for details [27]). The extracted growth exponent s in $\sqrt{\langle \phi^2 \rangle(x)} \propto L^s$ is smaller than 1/2, indicating a high probability of light remaining localized along the direction of longer correlation length, exhibiting a sub-diffusive transport regime (see Supplementary Material for details [27]).

In summary, we have demonstrated deterministic control over anisotropic branched flow of light by engineering programmable, spatially correlated disorder in nematic liquid crystals. This represents a fundamental advance: transforming branched flow from a passively observed wave phenomenon into an actively sculpted and reconfigurable transport regime. Our platform—enabled by photo-alignment techniques that offer micron-scale precision over the director field—allows the optical potential landscape to be tailored in both strength and anisotropy, providing unprecedented command over caustic formation and branching morphology. The experimental validation of a universal scaling law for the first-branch distance in anisotropic media underscores the role of engineered disorder as a governing factor in wave transport, bridging ballistic and diffusive propagation. Beyond scaling, we uncover that extreme spatial anisotropy triggers anomalous velocity diffusion, a symmetry-breaking process that dynamically confines light along preferential directions and leads to pronounced, tunable optical channeling. These findings reshape the understanding of wave scattering in correlated disorder, establishing anisotropy not merely as a parameter but as a design degree of freedom for controlling light in complex media.

This work is supported by National Key Research and Development Program of China (2023YFA1407104 and 2022YFA1405000), National Natural Science Foundation of China (12125504, 12274357, and 62475223), Shenzhen Science and Technology Program (JCYJ20240813145614019), Fujian Provincial Natural Science Foundation of China (2023J06011), and the “Hundred Talents Program” of the Chinese Academy of Sciences.

* yqlu@nju.edu.cn

† lujiachen@xmu.edu.cn

‡ jhjiang3@ustc.edu.cn

§ jimchen@xmu.edu.cn

- [1] A. Patsyk, U. Sivan, M. Segev, and M. A. Bandres, *Nature* **583**, 60 (2020).
- [2] A. Patsyk, Y. Sharabi, U. Sivan, and M. Segev, *Phys. Rev. X* **12**, 021007 (2022).
- [3] J. J. Metzger, R. Fleischmann, and T. Geisel, *Phys. Rev. Lett.* **105**, 020601 (2010).
- [4] S. Rotter and S. Gigan, *Rev. Mod. Phys.* **89**, 015005 (2017).
- [5] J. Garnier, A. Picozzi, and T. Torres, *Phys. Rev. Lett.* **134**, 223803 (2025).
- [6] M. Topinka, B. LeRoy, R. Westervelt, S. Shaw, R. Fleischmann, E. Heller, K. Maranowski, and A. Gossard, *Nature* **410**, 183 (2001).
- [7] M. Jura, M. Topinka, L. Urban, A. Yazdani, H. Shtrikman, L. Pfeiffer, K. West, and D. Goldhaber-Gordon, *Nat. Phys.* **3**, 841 (2007).
- [8] B. Liu and E. J. Heller, *Phys. Rev. Lett.* **111**, 236804 (2013).
- [9] D. Maryenko, F. Ospald, K. v. Klitzing, J. Smet, J. Metzger, R. Fleischmann, T. Geisel, and V. Umansky, *Phys. Rev. B* **85**, 195329 (2012).
- [10] S.-s. Chang, K.-H. Wu, S.-j. Liu, Z.-K. Lin, J.-b. Wu, S.-j. Ge, L.-J. Chen, P. Chen, W. Hu, Y. Xu, *et al.*, *Nat. Commun.* **15**, 197 (2024).
- [11] Y. Liu, K. Lin, Z. Liu, J. Qin, Q. Fu, P. Wang, and F. Ye, *Phys. Rev. Lett.* **135**, 143801 (2025).
- [12] H. Degueldre, J. J. Metzger, E. Schultheis, and R. Fleischmann, *Phys. Rev. Lett.* **118**, 024301 (2017).
- [13] J. Qin, Y. Liu, and F. Ye, *Laser & Photonics Reviews*, e01144 (2025).
- [14] H. Degueldre, J. J. Metzger, T. Geisel, and R. Fleischmann, *Nat. Phys.* **12**, 259 (2016).
- [15] J.-S. Gagnon, S. Lovejoy, and D. Schertzer, *Nonlin. Processes Geophys.* **13**, 541 (2006).
- [16] J. M. Dudley, F. Dias, M. Erkintalo, and G. Genty, *Nat. Photonics* **8**, 755 (2014).
- [17] M. V. Berry, *New J. Phys.* **7**, 129 (2005).
- [18] K. Jiang, T. Huang, R. Li, M. Yu, H. Zhuo, S. Wu, C. Zhou, and S. Ruan, *Phys. Rev. Lett.* **130**, 185001 (2023).
- [19] Y. Xu, M. Jin, J. Wang, S. Huang, and Q. Li, *Responsive Mater.* **2**, e20240020 (2024).
- [20] L.-L. Ma, C.-Y. Li, J.-T. Pan, Y.-E. Ji, C. Jiang, R. Zheng, Z.-Y. Wang, Y. Wang, B.-X. Li, and Y.-Q. Lu, *Light Sci. Appl.* **11**, 270 (2022).
- [21] H. Zhao and I. I. Smalyukh, *Nat. Mater.* (2025), 10.1038/s41563-025-02344-1.
- [22] B.-X. Li, V. Borshch, R.-L. Xiao, S. Paladugu, T. Turiv,

S. V. Shiyanovskii, and O. D. Lavrentovich, *Nat. Commun.* **9**, 2912 (2018).

[23] X. Wang, J. Jiang, J. Chen, Z. Asilehan, W. Tang, C. Peng, and R. Zhang, *Nat. Commun.* **15**, 1655 (2024).

[24] Z.-Y. Wang, Z. Zhou, H. Zhang, Y. Wei, H.-G. Yu, W. Hu, W. Chen, H.-T. Dai, L.-L. Ma, C.-W. Qiu, *et al.*, *eLight* **4**, 5 (2024).

[25] I.-C. Khoo and S.-T. Wu, *Optics and nonlinear optics of liquid crystals*, Vol. 1 (World Scientific, Singapore, 1993).

[26] E. P. Choate and H. Zhou, *Discrete Contin. Dyn. Syst.* **8**, 303 (2015).

[27] See Supplemental Material for a detailed description.

[28] L. Kaplan, *Phys. Rev. Lett.* **89**, 184103 (2002).

[29] T. Wei, P. Chen, M.-J. Tang, G.-X. Wu, Z.-X. Chen, Z.-X. Shen, S.-J. Ge, F. Xu, W. Hu, and Y.-Q. Lu, *Adv. Opt. Mater.* **8**, 1902033 (2020).

[30] B.-Y. Wei, P. Chen, S.-J. Ge, L.-C. Zhang, W. Hu, and Y.-Q. Lu, *Photon. Res.* **4**, 70 (2016).

[31] C. Meng, J.-S. Wu, and I. I. Smalyukh, *Nat. Mater.* **22**, 64 (2022).

[32] E. J. Heller, R. Fleischmann, and T. Kramer, *Phys. Today* **74**, 44 (2021).

[33] N. Bender, A. Goetschy, C. W. Hsu, H. Yilmaz, P. J. Palacios, A. Yamilov, and H. Cao, *Proc. Natl Acad. Sci.* **119**, e2207089119 (2022).

[34] S. Barkhofen, J. J. Metzger, R. Fleischmann, U. Kuhl, and H.-J. Stöckmann, *Phys. Rev. Lett.* **111**, 183902 (2013).

[35] H. E. Krogstad, J. Liu, H. Socquet-Juglard, K. B. Dysthe, and K. Trulsen, in *International Conference on Offshore Mechanics and Arctic Engineering*, Vol. 37440 (2004) pp. 285–295.